Cation ordering and the stability of fluorite-related phases in ZrO_2-$LnO_{1.5}$ systems: a phase diagram simulation study using Monte Carlo methods

1993 J. Phys.: Condens. Matter 5 4251

(http://iopscience.iop.org/0953-8984/5/25/015)

J. Phys.: Condens. Matter 5 (1993) 4251–4262. Printed in the UK

Cation ordering and the stability of fluorite-related phases in ZrO_2–$LnO_{1.5}$ systems: a phase diagram simulation study using Monte Carlo methods

Rita Khanna, T R Welberry and R L Withers

Research School of Chemistry, Australian National University, GPO Box 4, Canberra, ACT, 2601, Australia

Received 10 November 1992, in final form 22 February 1993

Abstract. We report Monte Carlo simulation results on cation ordering in a range of fluorite-related phases in various ZrO_2–$LnO_{1.5}$ systems. We restrict our attention to the face-centred cubic array of cations, assuming that the effect of the anion array upon the cation ordering can be simulated via effective cation–cation interactions. The basic interactions of the model include strongly repulsive nearest- (J_1) and next-nearest-neighbour (J_2) effective pair interactions and a three-spin interaction (J_3) term for the nearest neighbours. The ionic size difference between the two cation species is a measure of the strength of the interaction parameter J_2 and is a controlling factor for different kinds of ordering arrangement. While pyrochlore-type ordering is found to be stable for large values of J_2, the C-type phase is observed for small values of J_2. Both phases are found to coexist in the intermediate-parameter range. We report complete phase diagrams for two sets of interaction parameters computed within the framework of the 3D Ising model. The simulation results are consistent with electron and x-ray diffraction results on these mixed rare-earth oxide systems.

1. Introduction

The structure of pure zirconia, ZrO_2, is monoclinic from room temperature up to $\sim 1170\,^{\circ}C$, tetragonal between $\sim 1170\,^{\circ}C$ and $\sim 2370\,^{\circ}C$ and cubic (fluorite type) from $\sim 2370\,^{\circ}C$ up to the melting point at $\sim 2830\,^{\circ}C$. The 'stabilization' of the higher-temperature polymorphs of ZrO_2 via the addition of a relatively small amount ($\sim$ 5–20 mol.%) of the oxides of a variety of lower-valency metals—such as CaO, MgO or the lanthanide sesquioxides $LnO_{1.5}$—and subsequent quenching from sufficiently elevated temperatures ($\sim 1600\,^{\circ}C$) leads to anion-deficient materials with important ceramic and superionic conduction properties at elevated temperatures (Teufer 1962, de Vries *et al* 1979, Negita and Takao 1989). Increasing further the proportion of the lower-valency metal oxides typically leads to the stabilization of structure types not found in the pure ZrO_2 (although still closely related to the cubic fluorite-type parent phase and describable as compositional and displacively modulated variants thereof) such as the pyrochlore and C-type solid solution fields commonly reported at high temperatures ($> 1600\,^{\circ}C$) in various ZrO_2–$LnO_{1.5}$ systems (Allpress *et al* 1975, Rouanet 1971, Skaggs 1972, Bevan and Summerville 1979, Wadsley 1964).

It is important to note that non-stoichiometry in such systems is always taken up by the anion array, i.e. by the introduction of oxygen vacancies, while the nominally face-centred cubic (FCC) cation array always maintains its essential integrity. Such an observation suggests that cation–cation interactions (whether direct or mediated through the anions) play a crucial role. A further important characteristic feature of such simulated non-stoichiometric

0953-8984/93/254251+12$07.50

systems is that cation diffusion is many orders of magnitude lower than oxygen anion diffusion. At high temperatures they are all solid electrolytes, i.e. anion conductors with a molten (more or less completely disordered) anion array so that in a very real sense such systems at these temperatures can be thought of, and treated, as binary metallic alloys. When such materials are quenched the high-temperature metal atom ordering pattern is preserved. The oxygen ion array at low temperatures is a best possible response to this 'frozen-in' high-temperature cation array.

Given that the oxygen array is certainly very mobile at temperatures $> 1000\,^{\circ}C$, it is clear that the ordering in the quenched materials is strongly dependent upon the high-temperature ordering of the two cation species upon the much more rigid FCC metal atom array. In this paper, we propose a model to describe this cation ordering based upon a 3D Ising model (with the two cation species being represented by up and down spins and labelled as A and B) as is commonly done for binary alloy systems. We focus our attention upon the FCC array of cations and report the results of Monte Carlo simulation on cation ordering in a range of fluorite-related phases in various ZrO_2–$LnO_{1.5}$ systems. It is assumed that the effect of the anions upon the cation ordering can be simulated via effective cation–cation interactions.

The computer simulation was carried out using a 3D Ising model with the two cations being represented by up and down spins. The basic interactions of the model include a strongly repulsive nearest- (J_1) and next-nearest- (J_2) neighbour effective pair interactions and a three-spin interaction (J_3) term for the nearest neighbours (such an interaction was found to be necessary in order to obtain the commonly observed pyrochlore phase). While a repulsive J_1 ensures that there is no clustering of like atoms, the parameter J_2 is found to be the controlling factor for different kinds of ordering arrangement. The basic pairwise interaction between the cations is Coulombic in nature and therefore long ranged. However, instead of three pairwise interactions (E^{AA}, E^{AB} and E^{AB}), a single parameter $J = \frac{1}{4}(E^{AA}+E^{BB}-2E^{AB})$ has been used to represent the effective pair interaction (Richards and Cahn 1971). The parameter J is significant in magnitude up to a few near neighbours and is basically short ranged in character. We calculate here the complete phase diagrams for different strengths of the J_2 parameter and investigate the range and stability of various fluorite-related phases in these rare-earth mixed oxides.

2. The model

The model adopted here for cation ordering in these $(1-x)ZrO_2 \cdot xLnO_{1.5}$ systems consists of a binary cation system (A_xB_{1-x}) with atomic species A and B occupying a rigid FCC lattice. The configurational energy is determined, within the framework of the 3D Ising model, by the sum of effective pair interactions between the first- and second-nearest neighbours, denoted, respectively, by J_1 and J_2 (Sanchez and de Fontaine 1980, Allen and Cahn 1972). In the Ising spin language, a site i occupied by an A atom is represented by an up spin $S_i = 1$, and a site occupied by a B atom by a down spin $S_i = -1$. The Hamiltonian is equivalent to an Ising magnet in a magnetic field H:

$$H = J_1 \sum_{NN} S_i S_j + J_2 \sum_{NNN} S_i S_j - H \sum S_i \tag{1}$$

where the sum NN extends over all nearest-neighbour ($\frac{1}{2}\langle 110\rangle$) pairs and NNN over all next-nearest-neighbour ($\langle 100\rangle$) pairs. For antiferromagnetic ordering ($J_1 > 0$), minimization

of such a Hamiltonian gives rise to three distinct types of ground state ordering pattern dependent upon the ratio $\alpha = J_2/J_1$. These three patterns can be classified in terms of families of ordered structures and are labelled as (1) the $\langle 100 \rangle$ family for $\alpha < 0$, (2) the $\langle 1\frac{1}{2}0 \rangle$ family for $0 < \alpha < 0.5$, and (3) the $\langle \frac{1}{2}\frac{1}{2}\frac{1}{2} \rangle$ family for $\alpha > 0.5$ (Sanchez and de Fontaine 1982, Kanamori and Kakehashi 1978, Richards and Cahn 1971). In ZrO_2–$LnO_{1.5}$ systems, a pyrochlore type of ordering is commonly observed (space group $Fd3m$). Such pyrochlore-type ordering belongs to the $\langle \frac{1}{2}\frac{1}{2}\frac{1}{2} \rangle$ family. In their work on the ground state of ordered binary alloys, Richards and Cahn (1971) have pointed out that both $Fd3m$ and $R\bar{3}m$ structures have identical pair correlations out to infinity. It has also been shown by Clapp (1969) that the Ising model with pairwise interactions is generally highly degenerate. Some of this degeneracy can be removed if yet-higher-neighbour or multi-atom interactions are included in the Hamiltonian, as higher correlations among these structures are often different. In order for our model to produce exclusively pyrochlore-type ordering it is necessary to incorporate additional terms in the Hamiltonian.

The pyrochlore structure (stoichiometry $A_2B_2O_7$) can be described as a tunnel structure with a continuous 3D B_2O_6 framework of corner-sharing octahedra, the remaining A_2O atoms being in the tunnels (Knop *et al* 1965). In terms of the cation arrangement alone, an outstanding feature of this structure is the formation of two corner-sharing like-atom tetrahedra formed by nearest-neighbour atoms pointing along a $\langle 111 \rangle$ direction as shown in figure 1(*a*). While forming these tetrahedra, it becomes obvious that the remaining six nearest-neighbour atoms are always of the opposite type as ensured by both J_1 and J_2 being repulsive in character. In other words, three atoms forming the base of a tetrahedron are always of one type (either A or B). These like-atom tetrahedra point in a different $\langle 111 \rangle$ direction for each of the four sublattices of the FCC structure. These tetrahedra grow outwards with each corner atom acting as the apex of the two further corner-sharing like-atom tetrahedra. Using this as a basis, we introduce a three-spin interaction J_3 in the Hamiltonian. Equation (1) can then be written as

$$H + J_1 \sum_{\mathrm{NN}} S_i S_j + J_2 \sum_{\mathrm{NN}} S_i S_j + J_3 \sum_{m=1}^{2} \sum_{\mathrm{NN}} S_i S_j^m S_k^m \delta_{ijk} - H \sum S_i. \qquad (2)$$

J_3 is attractive (< 0) and $\delta_{ijk} = +1$ (-1) if the three nearest-neighbour spins i, j and k are all $+1$ (-1) and is zero otherwise. The twelve nearest neighbours of spin i are divided into two subsets. The $m = 1$ subset contains neighbouring spins belonging to the two tetrahedra and the remaining six neighbours are contained in the $m = 2$ subset. The second sum in the J_3 term is over the nearest-neighbour pairs of spins j and k. Note that the particular $\langle 111 \rangle$ direction necessary to define the $m = 1, 2$ subsets is different for each of the four sublattices. From figure 1, having chosen a $\langle 111 \rangle$ direction for a sublattice, the $\langle 111 \rangle$ directions associated with each of the remaining sublattices are automatically defined. Such an interaction is expected to promote pyrochlore-type cation ordering. It is to be noted that J_3 is rather specific to the present problem and is not a general three-spin interaction. The computer simulations were carried out within the following range of interaction parameters: $0 < J_1 \leqslant 1$; $0.5 < J_2 \leqslant 1$; and $-1 \leqslant J_3 < 0$.

3. The Monte Carlo simulations

We consider a system of $N = 4L^3$ spins on an FCC lattice with periodic boundary conditions. L was measured in units of the lattice constant a and has to be chosen such that the periodic

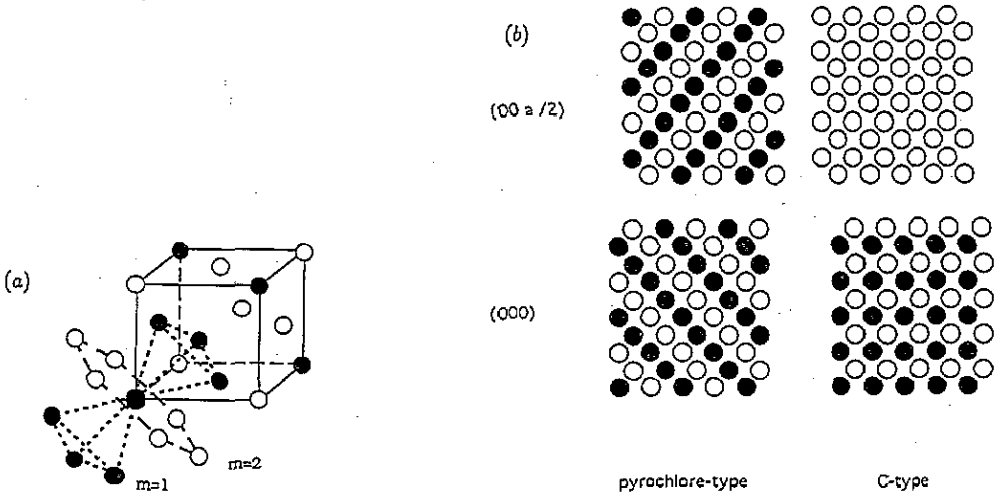

Figure 1. (*a*) One octant of the unit cell of the $Fd3m$ structure. The filled and the empty circles represent two different atomic species. Twelve nearest neighbours are divided in two subsets: six atoms belonging to the two tetrahedra are in subset $m = 1$, while the remaining six atoms are in the subset $m = 2$. (*b*) Cation arrangement in successive (001) layers in the pyrochlore-type and C-type ordering arrangements. While there is no change in the C-type ordering, the two cation species are interchanged in the next two layers of pyrochlore structure as compared to the ones shown above, indicating a repeat distance of $2a$.

boundary conditions are consistent with the expected ordered structures. We carried out most of our simulations for lattice sizes in the range $16 \leqslant L \leqslant 24$ ($16\,384 \leqslant N \leqslant 55\,296$). The simulations were performed using single spin-flip Glauber dynamics in the grand canonical ensemble, with the concentration c_B varying as a function of temperature and magnetic field. Starting from an initial configuration, which was chosen to be either disordered or perfectly ordered, the system was allowed to evolve according to the Metropolis algorithm (Binder 1979). The data were obtained for typically five to ten thousand Monte Carlo steps per site (MCSS).

Labelling the four sublattices of the unit cell of the FCC lattice as 1–4, we introduce the sublattice magnetizations m_ν,

$$m_\nu = (1/N) \sum_{i \in \nu} \langle S_i \rangle \qquad \nu = 1\text{–}4 \tag{3}$$

where $\langle\ \rangle$ is computed by taking time averages over different Monte Carlo runs. The total magnetization M is given by

$$M = m_1 + m_2 + m_3 + m_4 \tag{4}$$

and is related to the average concentration c_B of B atoms by

$$c_B = (1 + M)/2. \tag{5}$$

The cation ordering of the pyrochlore structure can be represented as an FCC superlattice with cell constant $2a$ (figure 1(*b*)). In order to define a pyrochlore order parameter m_p we require a minimum of eight sublattice magnetizations, four from one unit cell and four from

the next one (numbered from 5 to 8) along a ⟨100⟩ direction (labelled as i). The pyrochlore order parameter, m_p, can be expressed in terms of these m_ν as

$$m_p = \frac{1}{3}\sum_{i=1}^{3} m_p^i \tag{6}$$

where

$$m_p^i = [(m_1 - m_5) + (m_2 - m_6) + (m_3 - m_7) + (m_4 - m_8)]/8. \tag{7}$$

The order parameter, m_p, approaches unity in the pyrochlore phase and goes towards zero in other places. Another type of cation ordering often encountered in rare-earth mixed oxide systems is the C-type ordering pattern shown in figure 1(b). An order parameter for this structure, m_c, can be defined as

$$\begin{aligned} m_c^1 &= m_1 + m_2 + m_3 - m_4 & m_c^3 &= m_1 - m_2 + m_3 + m_4 \\ m_c^2 &= m_1 + m_2 - m_3 + m_4 & m_c^4 &= -m_1 + m_2 + m_3 + m_4. \end{aligned} \tag{8}$$

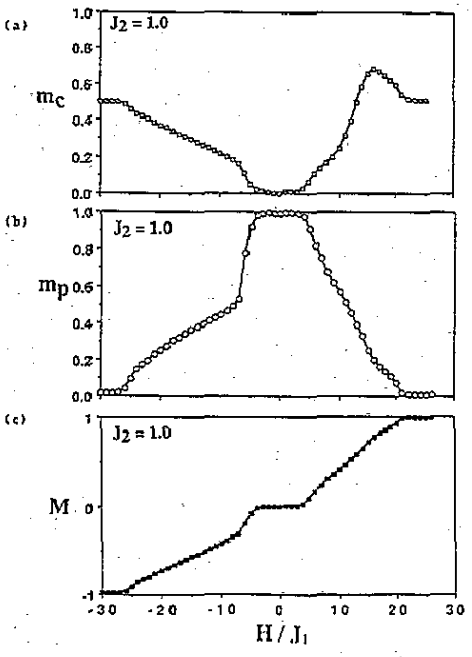

Figure 2. The average values of magnetization M (c), pyrochlore order parameter m_p (b) and order parameter for C-type ordering m_c (a) plotted versus magnetic field for next-nearest-neighbour interaction parameter $J_2 = 1.0$. The other parameters of the simulation were $J_1 = 1.0$, $J_3 = -0.5$ and $k_B T/J_1 = 1.5$.

Figures 2–4 show typical examples of 'raw data' of the Monte Carlo simulation for different sets of interaction parameters. The data were obtained in the grand canonical ensemble for $N = 16384$ and were averaged over 5000 MCSS after omitting the initial 100 MCSS to remove the effect of the initial conditions. The magnetization and two order parameters vary linearly in the disordered phase and deviate from this law in the region of long-range order. The pyrochlore-type ordering is present in all three sets of data and can be seen as the flat region around $M = 0$. With decreasing magnitude of the second-nearest-neighbour repulsion J_2, the pyrochlore region becomes narrower and narrower and

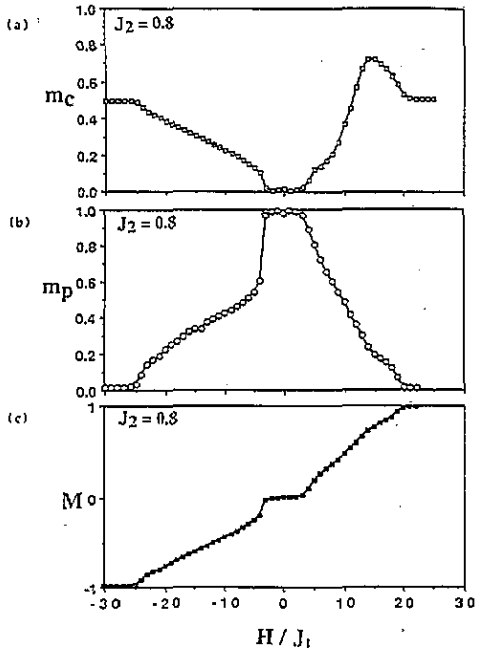

Figure 3. The average values of magnetization M (c), pyrochlore order parameter m_p (b) and order parameter for C-type ordering m_c (a) plotted versus magnetic field for the next-nearest-neighbour interaction $J_2 = 0.8$. The other parameters of the simulation were $J_1 = 1.0$, $J_3 = -0.5$ and $k_BT/J_1 = 1.5$.

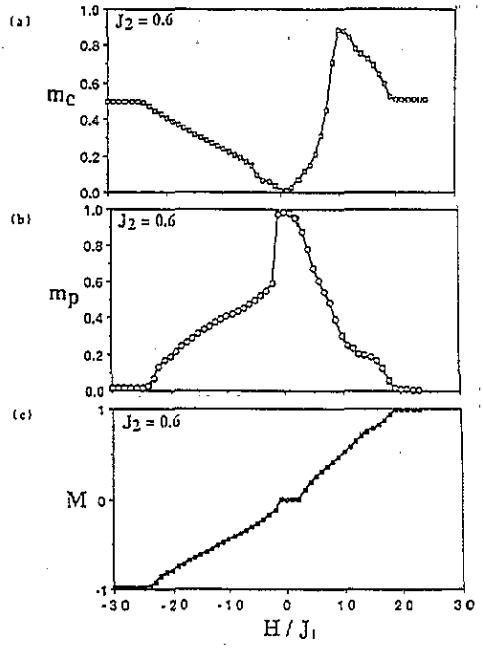

Figure 4. The average values of magnetization M (c), pyrochlore order parameter m_p (b) and order parameter for C-type ordering m_c (a) plotted versus magnetic field for the next-nearest-neighbour interaction $J_2 = 0.6$. The other parameters of the simulation were $J_1 = 1.0$, $J_3 = -0.5$ and $k_BT/J_1 = 1.5$.

a new phase starts making its appearance around $M = 0.5$ ($c_B = 0.75$) with a peak in the m_c order parameter. According to these preliminary Monte Carlo results, the relative stability and extent of pyrochlore- and C-type ordering can be controlled by the parameter J_2. Using figures 2–4 as a guideline for the choice of interaction parameters, complete phase diagram computations were carried out for the following two sets of parameters: (1) $J_1 = 1.0$, $J_2 = 1.0$, $J_3 = -0.5$ and (2) $J_1 = 1.0$, $J_2 = 0.7$ and $J_3 = -0.5$. The strength of J_3, which must be finite, affects mainly the stability of the C-type phase. A finite J_3 is however responsible for making the phase diagrams asymmetric (Styer *et al* 1986).

4. Phase diagram computations

Using the two sets of interaction parameters in the computation of phase diagrams, order parameter distribution functions were used to locate the phase boundary and to determine the order of the transition (Mouritsen 1984). $P(\phi)\,d\phi$ is defined as the probability that the order parameter will take on a value in the range $[\phi, \phi + d\phi]$. The distribution functions P for the magnetization M, and order parameters m_p and m_c were used in this analysis. Away from the transition, $P(\phi)$ is a sharp single-peaked function. But in the transition region $P(\phi)$ becomes a broad double-peaked function indicating that more than one phase is being populated. At the transition temperature, the two peaks have the same intensity. For a first-order transition, the peak separation tends to increase and then saturate with increasing lattice size. For a second-order transition, the two peaks move closer with increasing system

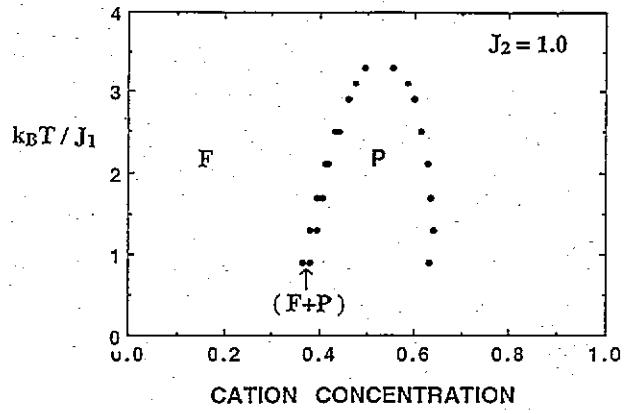

Figure 5. Temperature–composition phase diagram for the parameter set $J_1 = 1.0$, $J_2 = 1.0$, $J_3 = -0.5$. The temperature T in these plots stands for the parameter k_BT/J_1. Ordered structures are indicated.

size. $P(\phi)$ is therefore indispensable for locating the phase boundary and for determining the order of the transition.

4.1. Results for $J_1 = 1.0$; $J_2 = 1.0$; $J_3 = -0.5$

The phase diagram for the first parameter set obtained from the analysis of distribution function data is shown in figure 5. A dimensionless parameter k_BT/J_1 was used to represent the temperature. The phase diagram is dominated by pyrochlore-type (P) ordering in the central region of the phase diagram. This phase is stable over a wide temperature range and is surrounded on all sides by a disordered fluorite-type phase (labelled here as F). The F–P transition for $c_B < 0.5$ is very sharp and takes place over a very narrow magnetic field range. Figure 6(a) shows the order parameter $P(M)$ as a function of M for three different magnetic field values. As the field value is changed, $P(M)$ changes from a single-peak to a double-peak region indicating that two different states are being populated. As the field value is further increased, the second peak starts gaining in intensity and finally takes over completely. The double-peak region going over to a single peak indicates that the system has transformed completely from one state to another. For the sake of clarity, we have shown $P(M)$ values for only three magnetic fields. Simulations were carried out for a large number of points in the transition region. The coexistence region between the two phases is also very well defined and points towards a first-order transition. Figure 6(b) shows a plot of $P(M)$ versus M in the transition region for two different lattice sizes. As the lattice size increases, the two peaks move very slightly apart, thereby unambiguously confirming the phase transition from F to P to be of first order.

The P–F transition for $c_B > 0.5$ however is not so well defined and is not accompanied by sharp discontinuities in various order parameters (see figure 3). While the F–P transition could be conveniently located with even quite small lattice size simulations, it was found essential to use large lattice sizes ($L > 16$) for accurately locating the P–F transition. Figure 7(a) shows a plot of $P(M)$ versus M in the transition region for different field values and figure 7(b) a similar plot for two different lattice sizes. The size dependence of distribution function peaks which move closer with increasing lattice size indicates that the P–F transition is of second order. The P phase however is asymmetric around $c_B = 0.5$. This asymmetry is caused by the three-spin interaction term J_3 and disappears for $J_3 = 0$. In

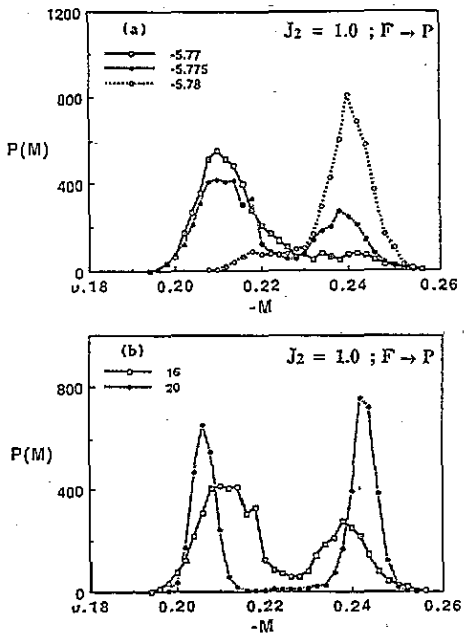

Figure 6. Plots of distribution function $P(M)$ versus M for $J_2 = 1.0$ and $k_BT/J_1 = 1.3$ for the F–P transition. (*a*) Plots of $P(M)$ for three different values of the field H/J_1. The magnitudes of H/J_1 are indicated against the plot symbol. The lattice size for these simulations was $L = 16$. (*b*) Plots of $P(M)$ for two different lattice sizes at $H/J_1 = -5.775$. The lattice size L is indicated against the plot symbol.

real systems, phase diagrams are generally asymmetric due to the concentration dependence of interaction parameters and the relative importance of higher-order interactions (Kikuchi *et al* 1980).

In this phase diagram, there is no evidence for the formation of C-type ordering around $c_B = 0.75$. Some short-range order does appear to be developing near $c_B = 0.8$ but it does not crystallize into a well defined phase as we could not detect any phase transition in that region. The phase diagram therefore consists solely of a disordered fluorite-type arrangement in conjunction with pyrochlore-type ordering in the central region of the phase diagram.

4.2. Results for $J_1 = 1.0$; $J_2 = 0.7$; $J_3 = -0.5$

The phase diagram for the second parameter set is shown in figure 8. There are some new features in this phase diagram. As expected from the average Monte Carlo data (figures 2–4) a reduced second-neighbour repulsion has resulted in compressing the region of stability of the pyrochlore-type phase around $c_B = 0.5$. The C-type ordering around $c_B = 0.75$ also becomes long ranged and develops into a well defined new phase. These phases are however restricted to a lower temperature range.

Now taking a closer look at each of the phase boundaries, the P phase is still surrounded on all sides by the disordered F phase. The F–P boundary for $c_B < 0.5$ continues to be very sharp and the coexistence region is again very well defined. A slight widening of the distribution function peaks with increasing lattice size once again unambiguously confirms

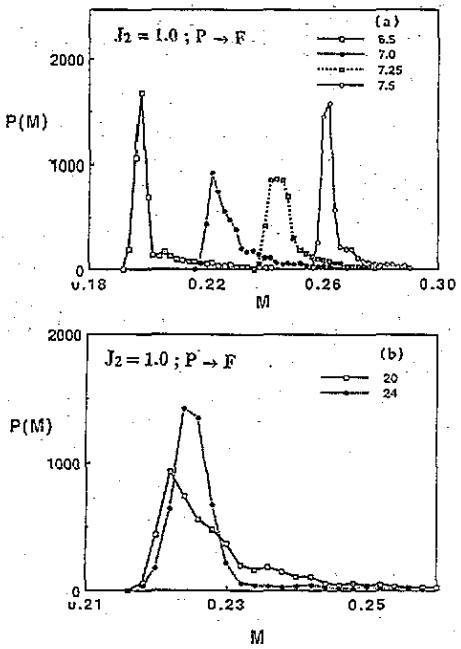

Figure 7. Plots of the distribution function $P(M)$ versus M for $J_2 = 1.0$ and $k_BT/J_1 = 1.3$ for the P–F transition. (*a*) Plots of $P(M)$ for three different values of the field H/J_1. The lattice size for these simulations was $L = 20$. (*b*) Plots of $P(M)$ for different lattice sizes at $H/J_1 = 7.25$.

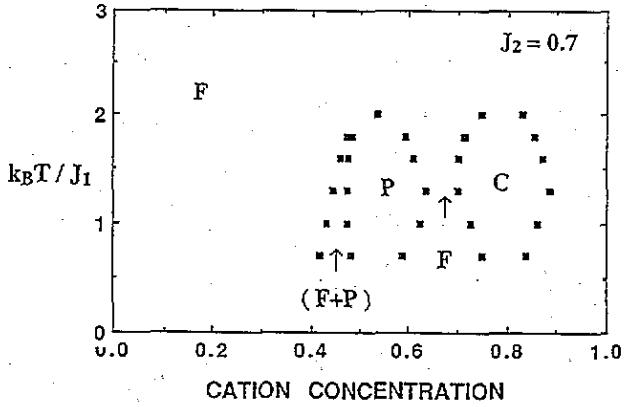

Figure 8. Temperature–composition phase diagram for the parameter set $J_1 = 1.0$, $J_2 = 0.7$, $J_3 = -0.5$. The temperature T in these plots stands for the parameter k_BT/J_1. Ordered structures and coexistence regions are indicated.

the transition from F to P to be of the first order. The P–F transition for $c_B > 0.5$ is better defined for this parameter set and could be comfortably located even for small lattice sizes. This transition is of second order. While the double-peak region has been used to identify the phase transition region, we have also used the criterion of distribution function peak broadening to locate the phase transition precisely. A broadening of the distribution

function peak corresponds to the critical slowing down near a transition (Landau and Binder 1978, Binder and Landau 1984) and provides invaluable information for systems where a double-peak region may be hard to identify. This is particularly true for second-order phase transitions.

The F–C phase transition is shown in figure 9. This transition is very well defined. Even though the double-peak region extends over a rather broad range of magnetic field values, the transition point could be unambiguously identified from the broadest distribution function peak. This transition is also of second order. The data for the C–F transition showed a great deal of scatter. The computations were carried out for larger lattice sizes ($L = 20, 24$ etc). Increasing the lattice size improved the scatter only very slightly. Despite the scatter, the transition can be located fairly accurately using the broadest distribution function peak criterion (lowest peak height) and this transition is also of second order (see figure 10). A narrowing of peaks coupled with increased peak height indicates that the system is moving away from the transition region towards a stable state.

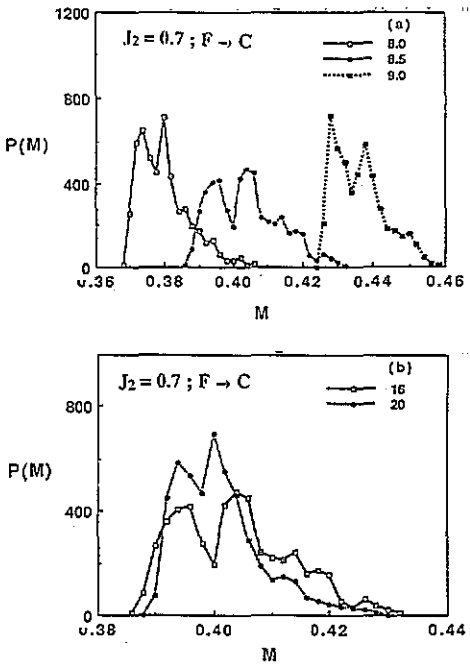

Figure 9. Plots of distribution function $P(M)$ versus M for $J_2 = 0.7$ and $k_B T/J_1 = 1.3$ for the F–C transition. (*a*) Plots of $P(M)$ for three different values of the field H/J_1. The lattice size for these simulations was $L = 16$. (*b*) Plots of $P(M)$ for two different lattice sizes at $H/J_1 = 8.5$.

5. Discussion and concluding remarks

The results of this investigation show that the strength of J_2 appears to be the driving force behind different ordering arrangements in these mixed rare-earth oxides. Pyrochlore-type

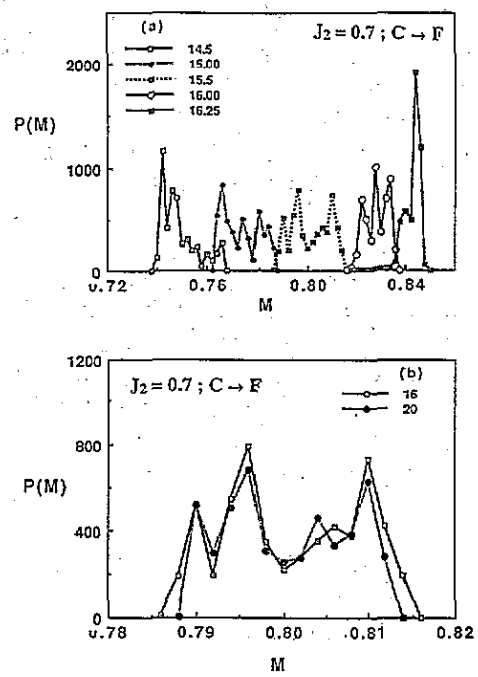

Figure 10. Plots of distribution function $P(M)$ versus M for $J_2 = 0.7$ and $k_B T/J_1 = 1.3$ for the C–F transition. (*a*) Plots of $P(M)$ for three different values of the field H/J_1. The lattice size for these simulations was $L = 16$. (*b*) Plots of $P(M)$ for two different lattice sizes at $H/J_1 = 15.5$.

cation ordering is favoured by large values of J_2. As the magnitude of J_2 decreases the region of stability of the pyrochlore phase decreases and C-type ordering starts making its appearance. As J_2 is further decreased the pyrochlore phase completely disappears and only C-type ordering remains. However J_1 and J_2 alone are not sufficient to stabilize these phases. The three-spin interaction term J_3 appears to play a very important role. While carrying out phase diagram simulations with only J_1 and J_2 interactions, it was extremely difficult to identify the phase boundaries of the pyrochlore phase even after increasing the lattice size beyond $L = 24$ ($N = 55\,296$) and carrying out simulations for more than 50 000 MCSS. After the addition of the J_3 term to the Hamiltonian, phase boundaries could be located to a good accuracy with $L = 16$ and data for typically 5000 MCSS. Apart from lifting the degeneracy with the $R\bar{3}m$ structure, J_3 tends to stabilize the pyrochlore phase and helps in defining the phase boundaries.

Another peculiar feature of the cation ordering in these oxides is the coexistence of the pyrochlore- and the C-type ordering patterns. A close look at figure 1(*b*) shows that while there is strong repulsion along (100) in the pyrochlore phase as indicated by two neighbours along this direction being always of the opposite type, the corresponding neighbours in the C-type phase are always of the same type. In fact the C-type cation ordering is the same as Cu_3Au ordering which requires an attractive next-nearest-neighbour interaction. With $J_2 > 0$, we should not observe a C-type phase at all. In the present case, the C-type phase is being stabilized by the three-spin-interaction term J_3. The dominance of J_3 over J_2 is also reflected in the presence of asymmetry in the $J_2 = 0.7$ phase diagram. In the $J_2 = 1.0$ phase diagram, the asymmetry is less pronounced due to the increased strength of the J_2

parameter.

Experimentally, the pyrochlore phase occurs in ZrO_2–$LnO_{1.5}$ when the ionic size difference between the lanthanide and zirconium ions is largest, i.e. for the larger rare-earth ions (La, Pr, Nd), whereas the C-type phase tends to occur for the smaller rare earths (Eyring 1979). Interpreting J_2 as a measure of this ionic size difference between the lanthanide and zirconium ions, the simulation results are consistent with experimental observations. Similarly, the widths of the simulated pyrochlore- and C-type regions are in good qualitative agreement with experimental observation. The simulations also give an idea of the cation arrangements in the off-stoichiometric regions. In the absence of long-range order there is a high degree of short-range order as indicated by the non-vanishing order parameters, and the cations cannot be assumed to be randomly arranged except at very high temperatures. Finally it is interesting to note that the $R\bar{3}m$ ordering pattern does occur experimentally in other fluorite-related systems such as $CaUO_4$. Although there are no such long-range ordered $R\bar{3}m$ phases in ZrO_2–$LnO_{1.5}$ systems, short-range ordering of this type has been observed in the ZrO_2–$PrO_{1.5}$ system (Withers *et al* 1992).

In this paper, we have developed a basic theoretical framework for cation ordering in rare-earth mixed oxides. This model is still very preliminary in nature. The three-spin interaction term was rather restrictive and could be made more general. Alternatively a four-body interaction may be more appropriate. The comparison with experimental results can undoubtedly be further improved by fine-tuning the strengths of various interaction parameters or by the addition of some more interactions in the Hamiltonian. These simulations are still of a preliminary nature and further improvement of the model and application to specific systems is in progress.

References

Allen M and Cahn J W 1972 *Acta Metall.* **20** 423

Allpress J G, Rossel H J and Scott H G 1975 *J. Solid State Chem.* **14** 264

Bevan D J M and Summerville E 1979 *Handbook of the Physics and Chemistry of Rare Earths* vol 3, ed K A Gschneider and L Eyring (Amsterdam: North-Holland) p 401

Binder K 1979 *Monte Carlo Methods in Statistical Physics* (Berlin: Springer)

Binder K and Landau D P 1984 *Phys. Rev.* B **30** 1477

Clapp P C 1969 *Proc. 3rd Bolton Landing Conf. AMIE*

de Vries K J, Van Jijk T and Burg-Graff A J 1979 *Fast Ion Transport in Solids* ed P Vashishta, J N Mundy and G K Shenoy (Amsterdam: North-Holland)

Eyring L 1979 *Handbook of the Physics and Chemistry of the Rare Earths* vol 3, ed K A Gschneider and L Eyring (Amsterdam: North-Holland) p 337

Kanamori J and Kakehashi Y 1978 *J. Physique Suppl.* **38** C7 274

Kikuchi R, Sanchez J M, de Fontaine D and Yamauchi H 1980 *Acta Metall.* **28** 651

Knop O, Brisse F, Meads R E and Bainbridge J 1965 *Can. J. Chem.* **46** 3829

Landau D P and Binder K 1978 *Phys. Rev.* B **17** 2328

Mouritsen O G 1984 *Computer Studies of Phase Transitions and Critical Phenomena* (New York: Springer) p 18

Negita K and Takao H 1989 *J. Phys. Chem. Solids* **50** 325

Richards M S and Cahn J W 1971 *Acta Metall.* **19** 1263

Rouanet A 1971 *Revue Int. Hautes Temp. Refract.* **8** 161

Sanchez J M and de Fontaine D 1980 *Phys. Rev.* B **21** 216

—— 1982 *Phys. Rev.* B **25** 1759

Skaggs S R 1972 *Sandia Laboratory Technical Report* SC-RR-72-0031, p 89

Styer D F, Phani M K, Stye A and Lebowitz J 1986 *Phys. Rev.* B **34** 3361

Teufer G 1962 *Acta Crystallogr.* A **15** 1187

Wadsley A D 1964 *Non-stoichiometric Compounds* ed L Mandelcorn (New York: Academic) p 99

Withers R L, Thompson J G, Barlow P J and Barry J C 1992 *Aust. J. Chem.* **45** 1375